Continuum absorption spectra in the far wings of the Hg $^1S_0 \rightarrow {}^3P_1$ resonance line broadened by Ar

Y. Sato, T. Nakamura, M. Okunishi, K. Ohmori, H. Chiba, and K. Ueda
Research Institute for Scientific Measurements, Tohoku University, Sendai 980-77, Japan
(Received 14 July 1995)

Absolute reduced absorption coefficients for the Hg resonance line at 253.7 nm broadened by Ar were determined between 390 and 430 K in the spectral range from 20 to 1000 cm^{-1} on the red wing and from 20 to 400 cm^{-1} on the blue wing. The resultant reduced absorption coefficients are in fair agreement with those obtained by Petzold and Behmenburg [Z. Naturtorsch. Teil A **33**, 1461 (1978)]. The observed $A\ ^3 0^+ \leftarrow X\ ^1 0^+$ spectrum in the spectral range from 80 to 800 cm^{-1} on the red wing agrees remarkably well both in shape and magnitude with the quasistatic line shape calculated using the potential-energy curves of the HgAr van der Waals molecule given by Fuke, Saito, and Kaya [J. Chem. Phys. **81**, 2591 (1984)], and Yamanouchi *et al.* [J. Chem. Phys. **88**, 205 (1988)]. The blue-wing spectrum is interpreted as the $B\ ^3 1 \leftarrow X\ ^1 0^+$ free-free transition of HgAr by a simulation of the spectrum using uniform semiclassical treatment for the free-free Franck-Condon factor. The source of the satellites on the blue wing is attributed to the phase-interference effect arising from a stationary phase-shift difference between the B- and X-state translational wave functions. The stationary phase-shift difference arises owing to the existence of a maximum in the difference potential between the B and X states. The repulsive branches of the potential-energy curves of HgAr for the X and B states have been revised to give excellent agreement between the observed and calculated spectra, both in shape and magnitude.

PACS number(s): 34.20.Cf, 33.70.Ca, 33.80.−b, 32.70.Jz

I. INTRODUCTION

The line shape in the far wings of the rare-gas broadened Hg $6s\ ^1S_0 \rightarrow 6p\ ^1P_1$ resonance line at 253.7 nm has for a long time been the subject of much experimental work [1–7]. In particular, the undulations or the satellite peaks superimposed on the far-wing continuum have attracted considerable attention. The nature of the blue-wing satellites of the Hg-Ar system has, however, been interpreted in contradictory ways: as a result of transitions from the free states [1,5] or from the bound states [2,7] of the Hg-Ar molecule.

The semiclassical line-shape theories have also been developed to describe the far-wing continuum including the satellite structures arising from the free-free transitions [8–10]. Petzold and Behmenburg [7] found, however, that their observed blue-wing spectra of Hg-Ar differ in shape and intensity level from the calculation by the unified Franck-Condon line-shape theory of Szudy and Baylis [10]. Petzold and Behmenburg therefore concluded that the Hg-Ar blue-wing spectra must be predominantly due to bound states and/or quasibound states existing within the rotational barrier of the effective potential.

On the other hand, laser spectroscopy combined with the free jet expansion technique has been applied to observe the bound-bound transitions of the Hg-Ar van der Waals (vdW) molecule in the vicinity of 253.7 nm [11–14]. These vdW studies have yielded much more accurate information about the potential wells for the ground $X\ 0^+$ and the excited $A\ 0^+$ and $B\ 1^+$ states relevant to the Hg-Ar transitions near 253.7 nm. The Hg-Ar potentials given by the vdW studies have been tested recently by the alignment effects studies for the photodissociation of the Hg-Ar molecule excited near 253.7 nm [15–17]. In their analysis of the alignment experiments, Segal and Harris [15] have reviewed the potentials given by the line-shape and the vdW experiments and proposed the potentials to be a combined form of the Morse potential from Fuke, Saito, and Kaya [11] and the C_6/R^6 potential. Laser spectroscopy of the Hg-Ar vdW molecule has been followed up most recently by Szajkowski, Krause, and Bobkowski [13] and Koperski, Atkinson, and Krause [14]. They have given different molecular constants for the X, A, and B states, which are slightly different from those of the former vdW experiments by Fuke, Saito, and Kaya [12] and Yamanouchi *et al.* [12]

We have reported previously the undulatory blue-wing spectra observed in absolute measurements of far-wing absorption spectra for the $6s\ ^1S_0 \rightarrow 6p\ ^1P_1$ resonance lines of Yb and Ba broadened by rare gases [18–20]. These undulations can be interpreted as arising from free-free transitions [20]. In this study, we have extended our experimental approach to the Hg (253.7 nm)–Ar system to follow up the earlier line-shape studies cited above. Our absolute measurements of the blue-wing spectra will then be analyzed using the uniform semiclassical approach for the free-free transitions based on the formalism of Bieniek and Streeter [21]. The main purpose of this study is to understand the nature of the blue-wing satellites in the light of improved information on the relevant potentials. It will be shown that the present treatment for the free-free transition can provide excellent agreement with the experiment in both shape and intensity level upon introducing a small modification of the potentials given from the vdW experiments in the region of their repulsive branches. We will discuss in some detail the mechanism responsible for the appearance of the blue-wing satellites and reasons why the generalized line-shape theory based on the random-phase approximation fails to explain the satellite peaks.

II. EXPERIMENT

We employed a classical double-beam absorption method using a Xe short-arc lamp as a continuum light source. The experimental setup and procedures were almost the same as those described in our previous paper [18]. Briefly, an absorption cell containing the Hg vapor and the Ar gas was placed in a test-beam section of the Mach-Zehnder interferometer. The cell, made of a quartz tube 100 cm long and 5 cm in diameter, with plane quartz windows at the ends, was operated at temperatures of 300–480 K. The perturber gas Ar is admixed in the cell at a pressure in the range 200–700 Torr. The light beam from a Xe short-arc lamp is divided into two: one passes through the absorption cell, while the other serves as a reference for the absorption. These two light beams and the interference beam, which is the superposition of these two beams, are alternately dispersed by a 50-cm Czerny-Turner spectrometer equipped with a grating of 1200 grooves/mm and are detected by a 1024-channel photodiode array. The overall resolution was about 0.1 nm. From the interference spectrum measured around the Hg resonance line, the number density of Hg atoms integrated over the line of sight, i.e., column density $N_{\mathrm{Hg}}l_a$, is determined. The absorption spectrum, in terms of the optical depth, is given by

$$k(\nu)l_a = -\ln[I_T(\nu)/I_R(\nu)], \tag{2.1}$$

where $I_T(\nu)$ and $I_R(\nu)$ are the relative spectral intensities of the test beam and the reference beam, respectively.

III. RESULTS

Absorption spectra of the Hg-Ar mixtures at 390 and 430 K for a variety of Ar pressures from 200 to 700 Torr are shown in Fig. 1 in terms of percentage absorption $[1-I_T(\nu)/I_R(\nu)]\times 100$ plotted against the wave-number shift Δ from the Hg $6s\ ^1S_0 \rightarrow 6p\ ^3P_1$ line at $\nu_0 = 39\,412.3$ cm^{-1}. The Ar pressures are from 200 to 700 Torr at intervals of 100 Torr. The column density $N_{\mathrm{Hg}}l_a$ was observed to depend weakly on the Ar pressure even at a constant cell temperature. $N_{\mathrm{Hg}}l_a$ was typically 1.69×10^{18} cm^{-2} at 390 K and 400 Torr, and 13.9×10^{18} cm^{-2} at 430 K and 400 Torr. The spectra on the red wing show small undulations over a spectral range of about -100 to -200 cm^{-1}. The peak positions of these undulations coincides with those reported by Kielkopf and Miller [5], who have attributed them to the bound vibrational levels of the upper electronic state. We will not be concerned with these small red-wing undulations, but with the gross features averaged over the undulations. The spectra on the blue wing show the prominent satellites SI and SII, the undulations well known from the literature.

Assuming that the far-wing spectrum consists of a superposition of the Hg-Ar and Hg-Hg components, we have

$$k(\Delta) = \gamma_{\mathrm{HgAr}}(\Delta)N_{\mathrm{Hg}}n_{\mathrm{Ar}} + \gamma_{\mathrm{HgHg}}(\Delta)N_{\mathrm{Hg}}^2 \tag{3.1}$$

and therefore

$$\frac{k(\Delta)l_a}{(N_{\mathrm{Hg}}l_a)^2} = \gamma_{\mathrm{HgAr}}(\Delta)\,\frac{n_{\mathrm{Ar}}}{N_{\mathrm{Hg}}l_a} + \frac{\gamma_{\mathrm{HgHg}}(\Delta)}{l_a}, \tag{3.2}$$

where $\gamma_{\mathrm{HgAr}}(\Delta)$ and $\gamma_{\mathrm{HgHg}}(\Delta)$ are the reduced absorption coefficients (RACs) at a wave-number shift Δ from the line

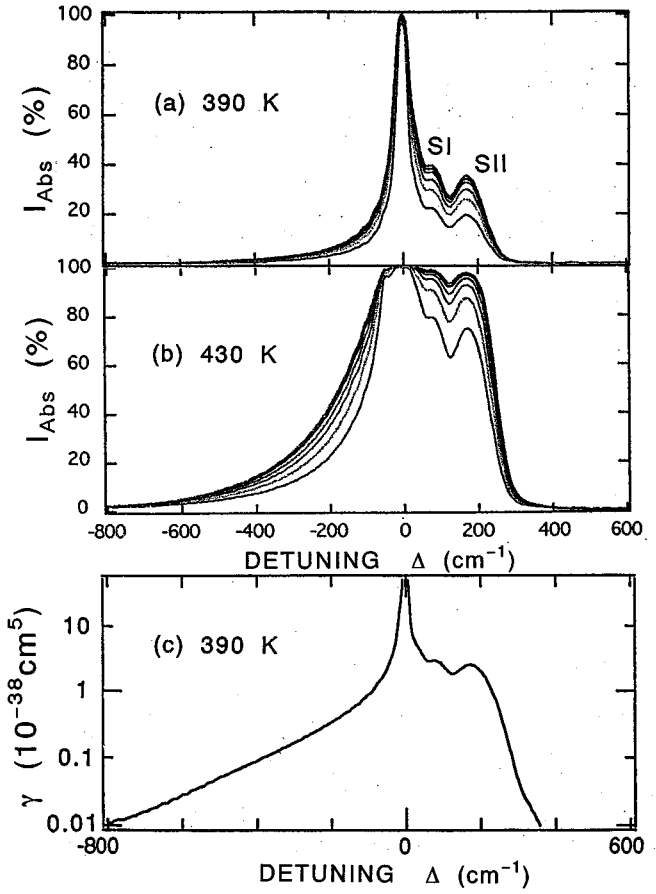

FIG. 1. (a) and (b) Absorption spectra, in terms of the percentage absorption $(1-I_T/I_R)\times 100$, in the vicinity of the Hg $6s\ ^1S_0-6p\ ^3P_1$ line at $\lambda = 253.7$ nm, plotted versus the wave-number shift from the Hg line. The cell temperatures are (a) 390 and (b) 430 K. The Ar pressures are 200, 300, 400, 500, 600, and 700 Torr. (c) Reduced absorption coefficients of Hg-Ar at 430 K derived from the spectra in (b).

center for the Hg-Ar and the Hg-Hg systems, respectively. Thus we can obtain γ_{HgAr} as a gradient and $\gamma_{\mathrm{HgHg}}/l_a$ as an intercept via the straight-line fit of the $kl_a/(N_{\mathrm{Hg}}l_a)^2$ versus $n_{\mathrm{Ar}}/N_{\mathrm{Hg}}l_a$ plot at each Δ in the spectral range covered in this study. The resultant RAC spectrum $\gamma_{\mathrm{HgAr}}(\Delta)$ is plotted in Fig. 1(c). The RACs determined at different temperatures will be given in Sec. IV together with the calculated ones. The RACs showed no significant dependence on temperature within the present temperature variation from 390 to 430 K. The absolute RACs from the present measurements are in good agreement with those of Behmenburg and co-workers [3,4,7]. We focus here on the results of $\gamma(\Delta)_{\mathrm{HgAr}}$ for the Hg-Ar molecule. The results of $\gamma_{\mathrm{HgHg}}(\Delta)$ will be reported elsewhere.

IV. DISCUSSION

A. Red-wing spectrum

The present red-wing spectrum has been obtained at negative detunings smaller than -20 cm^{-1}, where the spectrum can be assigned to the $A\ ^3\Sigma_0^+ \leftarrow X\ ^1\Sigma_0^+$ transition. Fuke, Saito, and Kaya [11] and Yamanouchi *et al.* [12] have found that

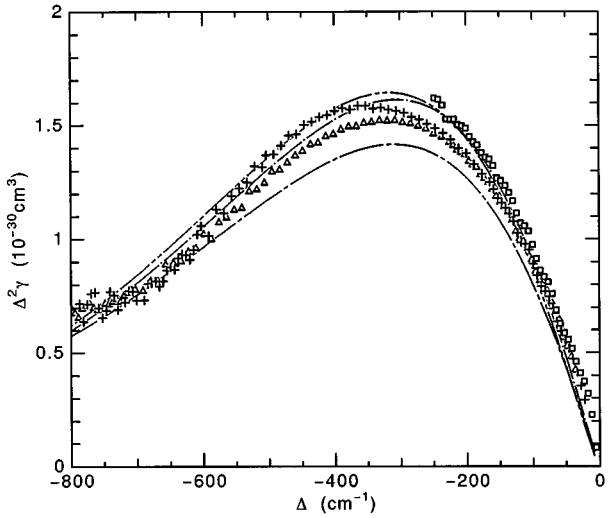

FIG. 2. Reduced absorption coefficient multiplied by the square of the wave-number shift from the Hg(253.7 nm) line center plotted against the wave-number shift for the red-wing $A \leftarrow X$ transition of Hg-Ar. The experimental results at 390 K (□), 415 K (+), and 430 K (△) are compared with the QST calculations for 415 K. The QST calculations are shown for the Morse potentials by Yamanouchi *et al.* Ref. [12] (— — —), by Fuke, Saito, and Kaya [11] (–·–), and by Koperski, Atkinson, and Krause [14] (— — —).

Morse functions are appropriate to describe the potential wells of the X, A, and B states of the Hg-Ar molecule. We compare the observed red-wing spectra with the quasistatic line shapes calculated for the $A \leftarrow X$ transition using the Morse potentials determined by the vibrationally resolved spectroscopy of the Hg-Ar molecule [11,12,14]. The calculation of the quasistatic wing is based on the classical quasistatic theory (QST) [22,23], which gives the RAC γ as a function of the detuning Δ as

$$\gamma(\Delta) = \frac{(2\pi\alpha)^2 a_0 (f_a/3) R_\Delta^2}{\Delta V'_{A-X}(R_\Delta)} \exp\left[-\frac{V_X(R_\Delta)}{k_B T} \right], \quad (4.1)$$

where R_Δ is the Hg-Ar distance that satisfies the classical Franck-Condon relation

$$\Delta = V_A(R_\Delta) - V_X(R_\Delta) - \nu_0, \quad (4.2)$$

α ($=\frac{1}{137}$) is the fine-structure constant, a_0 is the Bohr radius, f_a is the oscillator strength for the Hg atomic line (equal to 0.0255 [24]), and $\Delta V'_{A-X}(R)$ is the first derivative of the difference potential $V_A(R) - V_X(R)$ with respect to R.

The red-wing spectra observed at $T = 390$, 415, and 430 K are plotted in Fig. 2 in terms of the RAC multiplied by the square of the wave-number shift from line center and compared with three QST curves calculated for $T = 415$ K using different potential curves. The observed spectra at these three different temperatures show small discrepancies with each other. However, these differences may not be significant, considering the present experimental accuracy. We regard the results as an indication of no significant temperature dependence within the present small temperature variation.

The three QST curves at Fig. 2 correspond to the Morse potentials from the spectroscopic constants of Fuke, Saito, and Kaya [11], Yamanouchi *et al.* [12], and Koperski *et al.* [14] The Morse parameters deduced from their spectroscopic constants are listed in Table I. The Morse potentials by Fuke, Saito, and Kaya and Yamanouchi *et al.* give almost similar γ's while those by Koperski, Atkinson, and Krause give γ's a little smaller. All of these QST curves are in good agreement with the present experimental results in both shape and magnitude, as seen in Fig. 2. Note that the plot of $\Delta^2\gamma$ accentuates a small difference in γ at larger absolute detunings. It is therefore concluded that the QST values of γ calculated from the Morse potentials by Fuke, Saito, and Kaya and Yamanouchi *et al.* agree remarkably well with the experimental data for red-wing detunings larger than 80 cm^{-1}. Discrepancies in γ between theory and experiment grow larger rather for $|\Delta|$ smaller than 80 cm^{-1}. This may be attributed, as has been discussed by Segal and Harris [15], to the fact that the Morse potential converges to zero too quickly for a correct description of the long-range van der Waals interaction.

TABLE I. Summary of potential parameters. $\beta_1{}^b$, $\beta_1{}^c$, and $\beta_1{}^d$ are calculated assuming the Morse relation $\beta_1 = 0.1218\omega_e(\mu/D_e)^{1/2}$, where β_1 is in units of Å^{-1}, ω_e and D_e in cm^{-1}, and μ in amu.

State	D_e (cm^{-1})	R_e (Å)	β_1 (Å^{-1})	β_2 (Å^{-1})
$X\ ^1\Sigma_0^+$	143[a], 142[b]	4.02[a], 4.01[b]	1.40[a], 1.39[b]	3.02[a]
	143[c], 134[d]	3.99[c], 3.99[d]	1.38[c], 1.50[d]	
$A\ ^3\Sigma_0^+$	377[a], 369[b]	3.36[a], 3.38[b]	1.49[a], 1.45[b]	
	377[c], 362[d]	3.36[c], 3.38[d]	1.49[c], 1.54[d]	
$B\ ^3\Pi_1$	63[a], 67[b]	4.62[a], 4.66[b]	1.13[a], 1.04[b]	2.22[a]
	63[c], 67[d]	4.70[c], 4.64[d]	1.02[c], 1.09[d]	

[a]Parameters used in this work.
[b]Reference [11].
[c]Reference [12]. D_e is calculated as $D_e = D_0 + \omega_e/2$ using ω_e and D_0 in Ref. [12].
[d]Reference [14].

As will be discussed later, we modify the ground-X-state potential in order to make a reasonable simulation for the blue-wing $B \leftarrow X$ line-shape data. We assume an extended Morse function for the $X\ ^1\Sigma_0^+$ state potential

$$V(R) = a\left[e^{-\beta_2 \hat{R}} - \frac{\beta_2}{\beta_1} e^{-\beta_1 \hat{R}} \right], \quad (4.3)$$

where $\hat{R} = R - R_e$ and the parameter a is related to the well depth D_e as $D_e = -a(1 - \beta_2/\beta_1)$. While keeping D_e and R_e at the values given by Yamanouchi *et al.*, we determined β_1 and β_2 so that we obtained a quasistatic line shape in good agreement with the observed red-wing spectrum. The X-state potential thus determined is quite similar to the Morse potential of Yamanouchi *et al.* in the attractive branch, but has a steeper dependence on R in the repulsive branch (see Fig. 3). The potential parameters are summarized in Table I. The QST curve of $\Delta^2\gamma$ calculated from the modified X-state potential and the A-state Morse potential by Yamanouchi *et al.*, though it is not shown in Fig. 2 to avoid complexity, lies between the curves corresponding to the Morse potentials of Fuke, Saito, and Kaya and Koperski, Atkinson, and Krause.

B. Blue-wing spectrum

The blue-wing spectrum at detunings larger than 20 cm^{-1} corresponds to the $B \leftarrow X$ transition. If the Morse potentials of Yamanouchi *et al.* are extended to the range above the dissociation limit, the difference potential $\Delta V_{B-X}(R) = V_B(R) - V_X(R) - \nu_0$ gives a maximum $\Delta_M \sim 600$ cm^{-1} at $R \sim 3.1$ Å. This maximum appears because the repulsive branch of V_X is steeper than that of V_B. Though the prominent satellite observed in the blue wing is obviously due to the existence of such a maximum in ΔV_{B-X}, its height $\Delta_M \sim 600$ cm^{-1} is too high considering that the peak of the outermost satellite SII appears at $\Delta \sim 170$ cm^{-1} (see Fig. 1). Therefore, the repulsive branch of V_X must have a steeper dependence on R and/or that of V_B must depend on R less than expected from the Morse potentials of Yamanouchi *et al.* This is the reason why we have assumed the extended Morse function for V_X. In order to modify the repulsive part of V_B, we use an extended Morse form and further introduce a function $f(R)$ [25]

$$V_B(R) = a\left[e^{-\beta_2 \hat{R}} - \frac{\beta_2}{\beta_1} e^{-\beta_1 \hat{R}} \right] f(R), \tag{4.4}$$

with

$$f(R) = 1 - b_1 \exp\left[-\left(\frac{R - b_2}{b_3} \right)^2 \right]. \tag{4.5}$$

The b parameters in $f(R)$ are chosen so that the factor $f(R)$ modifies only the repulsive part of V_B and changes neither the well depth nor the attractive part of V_B. The maximum Δ_M of ΔV_{B-X} is sensitive to the b parameters in $f(R)$. The values of the b parameters finally chosen are $b_1 = 0.43$, $b_2 = 2.96$ Å, and $b_3 = 0.635$ Å. The other potential parameters for the B state employed to simulate the blue-wing spectrum are listed in Table I. Figure 3 shows the potential-energy curves we used to calculate the red- and blue-wing spectra. The resultant difference potential ΔV_{B-X} is also shown in Fig. 3. ΔV_{B-X} has a maximum $\Delta_M \simeq 220$ cm^{-1} at $R \simeq 3.6$ Å.

We have calculated the blue-wing line shape assuming that the free-free transitions between the $B\ ^3\Pi$ and $X\ ^1\Sigma^+$ states are responsible for this continuum. The calculations of the RAC at temperature T were performed according to [26]

$$\gamma_T(\Delta) = 8\pi^4 \alpha^2 (2 f_a/3) \frac{hc}{Q_T} \times \int_0^\infty \left[\sum_l (2l+1) |\langle \Psi_B | \Psi_X \rangle|^2 \right] \exp\left(-\frac{E}{k_B T} \right) dE, \tag{4.6}$$

where Q_T is the translational partition function, l the angular-momentum quantum number of the relative nuclear motion, $\langle \Psi_B | \Psi_X \rangle$ the overlap integral of the nuclear translational wave functions, and E the initial kinetic energy. We have used the uniform-semiclassical formula by Bieniek and Streeter [21] to calculate the free-free Franck-Condon overlap integrals.

When the difference potential ΔV_{B-X} has a maximum at $R = R_0$ as shown in Fig. 3, two Condon points R_1 and R_2 ($R_1 < R_0 < R_2$) can contribute to the transition for a given

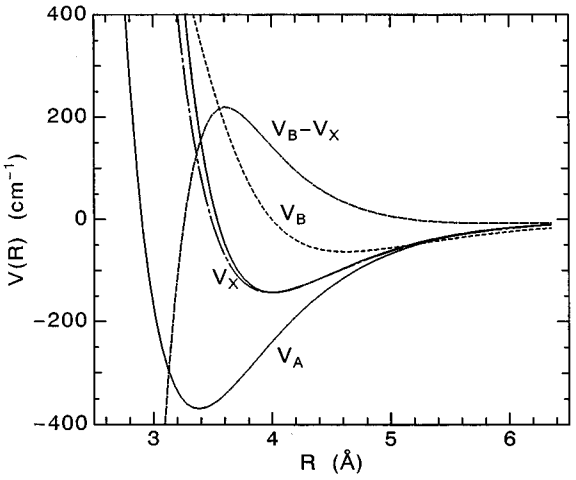

FIG. 3. Hg-Ar potentials used in this work. The potentials of the excited states V_A and V_B are displaced by their asymptotic value ν_0. V_A is the A state Morse potential with the parameters from Ref. [12]. V_B is the modified B state potential introduced in this study. Two curves are shown for the X-state potential: One is the modified X state potential of an extended Morse form (solid line) and the other is the Morse potential by Yamanouchi *et al.* [12]. The latter is plotted by a chain line for comparison. The difference potential $\Delta V_{B-X} = V_B - V_X - \nu_0$ is also shown, where V_B and V_X are the modified potentials introduced in this study.

absorption wavenumber. Let l_{nM} ($n = 1$ or 2) be the maximum angular momentum that allows the collision pair to approach within the Condon point R_n

$$l_{nM} = \mathrm{Int}\left\{ k_E R_n \left[1 - \frac{V_X(R_n)}{E} \right]^{1/2} - \frac{1}{2} \right\}, \tag{4.7}$$

where Int denotes integer part of and $k_E = \sqrt{2\mu E}/\hbar$ is the initial kinetic wave number. Then the summation over l in Eq. (4.6) must be divided into two parts

$$\sum_l (2l+1) |\langle \Psi_B | \Psi_X \rangle|^2 = q_{12} + q_2, \tag{4.8}$$

with

$$q_{12} = \sum_{l=0}^{l_{1M}} (2l+1) |T_1 + T_2|^2 \tag{4.9}$$

and

$$q_2 = \sum_{l=l_{1M}+1}^{l_{2M}} (2l+1) |T_2|^2. \tag{4.10}$$

The q_{12} term includes the contributions of both Condon points while the q_2 term contains a contribution only from the outer Condon point R_2. According to the uniform-semiclassical expression by Bieniek [21,27],

$$T_n = \pi \left(\frac{\hbar^2}{2\mu |\Delta V''(R_n)| k_n^2} \right)^{1/3} [\cos \beta_n \ \mathrm{Ai}(-z_n) - (-1)^n \sin \beta_n \ \mathrm{Bi}(-z_n)], \tag{4.11}$$

where $\mathrm{Ai}(-z)$ and $\mathrm{Bi}(-z)$ are the regular and irregular homogeneous Airy functions respectively. β_n and z_n are related to the phase-shift difference $\Delta\phi_n$ evaluated at the Condon point R_n

$$\beta_n=\Delta\phi_n+\tfrac{2}{3}|z_n|^{3/2}, \tag{4.12}$$

$$z_n=\pm\left|\frac{(\Delta\phi_n'')^3}{2(\Delta\phi_n''')^2}\right|^{2/3}, \tag{4.13}$$

$$\Delta\phi_n=\int_{R_B^t}^{R_n}k_B(R)dR-\int_{R_X^t}^{R_n}k_X(R)dR. \tag{4.14}$$

R_X^t and R_B^t are the classical turning points on the X and B states, respectively, and $k(R)$ is the semiclassical local wave number

$$k_X(R)=k_E\left[1-\frac{V_X(R)}{E}-\left(\frac{l+\frac{1}{2}}{k_ER}\right)^2\right]^{1/2}, \tag{4.15}$$

$$k_B(R)=k_E\left[1-\frac{V_B(R)-(\nu_0+\Delta)}{E}-\left(\frac{l+\frac{1}{2}}{k_ER}\right)^2\right]^{1/2}. \tag{4.16}$$

The above two local wave numbers have the same value at the Condon point

$$k_X(R_n)=k_B(R_n)=k_n. \tag{4.17}$$

This is the semiclassical equivalent to the classical Franck-Condon relation in Eq. (4.2) under the Q-branch approximation [28]. For the derivatives of the phase difference in Eq. (4.13), the following approximations are used [8]:

$$|\Delta\phi_n''|=\frac{\mu}{\hbar^2k_n}|\Delta V_n'|,\quad |\Delta\phi_n'''|=\frac{\mu}{\hbar^2k_n}|\Delta V_n''|, \tag{4.18}$$

where $\Delta V_n'=\Delta V'(R_n)$ and $\Delta V_n''=\Delta V''(R_n)$.

We have examined another uniform-semiclassical expression for the q_{12} term. This expression includes only the second derivative of the phase difference $\Delta\phi_n$ [21]

$$q_{12}=\sum_{l=0}^{l_{1M}}(2l+1)(U_a^2+U_b^2), \tag{4.19}$$

$$U_a=(u_1+u_2)\zeta^{1/4}\cos[\tfrac{1}{2}(\Delta\phi_1+\Delta\phi_2)]\mathrm{Ai}(-\zeta), \tag{4.20}$$

$$U_b=(u_1-u_2)\zeta^{1/4}\sin[\tfrac{1}{2}(\Delta\phi_1+\Delta\phi_2)]\mathrm{Bi}(-\zeta), \tag{4.21}$$

$$u_n=\frac{\pi}{\sqrt{2}}k_n^{-1}|\Delta\phi_n''|^{-1/2}=\frac{\pi\hbar}{(2\mu k_n|\Delta V_n'|)^{1/2}}, \tag{4.22}$$

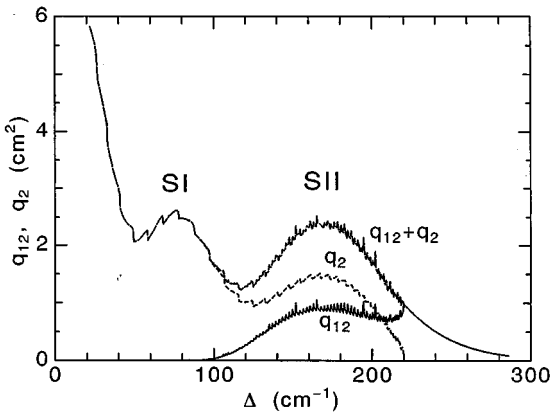

FIG. 4. Dependence of the partial Franck-Condon factors, the q_1 and q_2 terms, on the wave-number shift Δ for the Hg-Ar $B\leftarrow X$ transition. The initial kinetic energy is 345 cm^{-1}.

where $\zeta=(\mu/\hbar^2k_0)^{2/3}|\Delta V_0''|^{-1/3}(\Delta_M-\Delta)$ for $\Delta\geqslant\Delta_M$, $\zeta=|\frac{3}{4}\Delta\phi_{12}|^{2/3}$ for $\Delta<\Delta_M$, $k_0=k_X(R_0)$, $\Delta V_0''=\Delta V''(R_0)$, and $\Delta\phi_{12}=\Delta\phi_2-\Delta\phi_1$.

Equation (4.19) gives almost the same numerical results as Eq. (4.9). We have used Eq. (4.19) for the present analysis. Figure 4 shows the Δ dependence of the q_{12} and q_2 terms for an initial kinetic energy $E=345$ cm^{-1}. This value of E corresponds to the mean velocity for $T=390$ K, i.e., one of the temperatures at which our measurements have been made. As seen in the figure, the q_{12} term is important at the outermost SII satellite region including the antistatic wing beyond Δ_M. In most of the regions of Δ smaller than Δ_M, the q_2 term dominates over the q_{12} term. Moreover, the q_2 term shows undulatory structure; at least two peaks can be clearly seen. The main satellite SII is the additive superposition of the q_{12} and q_2 terms, while the satellite SI at about 80 cm^{-1} comes from the q_2 term. For Δ's smaller than 100 cm^{-1}, the q_{12} term vanishes. This is because the potential height at the inner Condon point $V_X(R_1)$ is higher than the initial kinetic energy and therefore the Hg-Ar pair cannot reach R_1. In these regions, the summation over l in the q_2 term extends from 0 to l_{2M}.

The oscillation in q_2 comes from the fact that the phase difference $\Delta\phi_2$ in Eq. (4.14) has a maximum at some l, say l^*. The main contribution to q_2 comes from the stationary phase difference $\Delta\phi_2(l^*)$. If the asymptotic form of the Airy functions are used in Eq. (4.11), we have

$$T_2\simeq\left(\frac{\pi\hbar^2}{2\mu|\Delta V_2'|k_2}\right)^{1/2}\sin\left[-\Delta\phi_2+\frac{\pi}{4}\right]. \tag{4.23}$$

Equation (4.23) is a good approximation for the uniform-semiclassical expression in Eq. (4.11) for most of the range of Δ, $0<\Delta\leqslant 0.9\Delta_M$, except the region close to Δ_M. $\Delta\phi_2$ in Eq. (4.14) may be approximated as

$$\Delta\phi_2(l)\simeq\frac{1}{h\nu}\int_{b_l}^{R_2}\frac{\Delta V(R)-\Delta}{\sqrt{R^2-b_l^2}}R\,dR, \tag{4.24}$$

where $b_l=(l+\frac{1}{2})/k_E$ is the impact parameter corresponding to the angular momentum l. Equation (4.24) implies that if

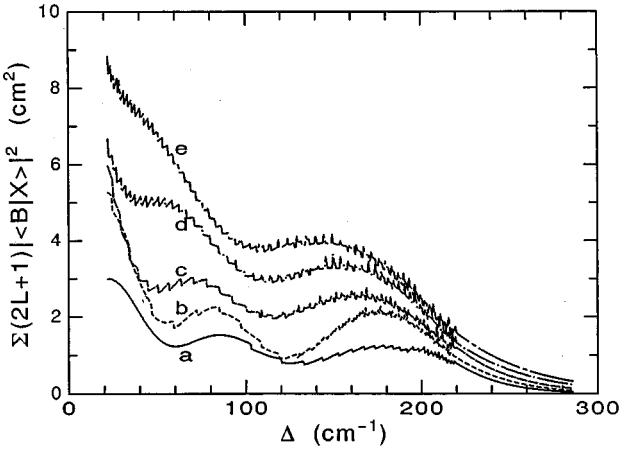

FIG. 5. Δ dependence of the free-free Franck-Condon factor $q_{12}+q_2$ for various initial kinetic energies: *a*, 100 cm^{-1}; *b*, 260 cm^{-1}; *c*, 500 cm^{-1}; *d*, 1000 cm^{-1}; and *e*, 1500 cm^{-1}.

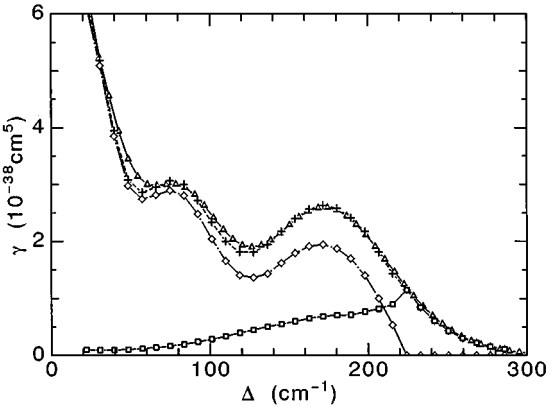

FIG. 6. Reduced absorption coefficients of Hg-Ar at 390 K versus the blue-wing shift of the wave number from the Hg(253.7 nm) line center: Δ, from the experiment; +, from the calculation. The calculated spectrum is decomposed into components corresponding to the q_{12} term (◇) and the q_2 term (□).

$\Delta V(R)$ has a maximum within R_2, it is possible for $\Delta\phi_2$ to have a maximum as a function of l. This is exactly the case for the blue-wing satellite, because $\Delta V_{B-X}(R)$ has a maximum Δ_M at $R=R_0$ ($R_0<R_2$). One may employ the stationary-phase approximation instead of the random-phase approximation by replacing the summation by the integration over l in Eq. (4.10) to obtain a smoothly varying term and an oscillatory term

$$q_2 \simeq \bar{q}_2 - \frac{\pi^{3/2}\hbar^2(l^*+\frac{1}{2})}{2\mu|\Delta V_2'|[k_2|d^2\Delta\phi_2/dl^2|^{1/2}]_{l^*}} \cos[2\Delta\phi_2(l^*) - \pi/4]. \quad (4.25)$$

Since $\Delta\phi_2(l^*)$ depends on Δ, q_2 oscillates as a function of Δ. This type of oscillation mechanism is quite parallel to the one that has been employed to interpret the oscillations in the integrated cross sections of inelastic atomic collisions arising from curve crossing [29,30].

The upper limit of the integration over E in Eq. (4.6) can safely be taken to be $6k_BT$ to calculate γ_T for a given temperature T. Figure 5 shows the total Franck-Condon factor $q_{12}+q_2$ calculated for several different initial energies E. As E increases, the positions of the satellites shift towards lower Δ. However, the shift is relatively small within most of the effective range of E, so that the oscillatory structure will not be smeared out by Boltzmann averaging over the energy E. We have carried out the integration over E in Eq. (4.6) to calculate the RAC, $\gamma_T(\Delta)$, for a given temperature T. The calculated $\gamma_T(\Delta)$ for the blue wing of Hg-Ar at $T=390$ K is compared with the experimental one in Fig. 6. Decomposition of the calculated $\gamma_T(\Delta)$ into components corresponding to the q_{12} and q_2 terms is also shown in Fig. 6. The calculated $\gamma_T(\Delta)$ shows excellent agreement with the experiment in both shape and intensity level. The oscillations seen in q_2 for a given initial energy E (Fig. 6) are not smeared out even after Boltzmann averaging. The positions of the satellites in $\gamma_T(\Delta)$ at a temperature T are well represented by the peaks seen in Fig. 6 for $q_{12}+q_2$, at an energy $E=4k_BT/\pi$ corresponding to a mean velocity $\bar{v}=\sqrt{8k_BT/\pi\mu}$ at that temperature. The maximum Δ_M of the difference potential ΔV_{B-X} is located at a detuning wave number beyond the outermost satellite peak where the intensity is about 45% of the peak satellite intensity.

V. CONCLUSION

We have employed the classical double-beam absorption-dispersion method to determine the absolute reduced absorption coefficient $\gamma_T(\Delta)$ for the far wings of the Hg $6s\ ^1S_0 \rightarrow 6p\ ^3P_1$ resonance line broadened by Ar at temperatures from 390 to 430 K. The resultant $\gamma_T(\Delta)$'s are in reasonable agreement with those by Behmenburg and co-workers [3,4,7]. The observed $A \leftarrow X$ red-wing spectrum in a wave-number shift between 80 and 800 cm^{-1} from the line center agrees remarkably well in both shape and magnitude with the quasistatic line shape calculated using the Morse potentials determined from vibrationally resolved spectroscopy of the Hg-Ar molecule [11,12].

The repulsive parts of the potential-energy curves for the X and B states are determined from the analysis of the blue-wing spectrum using the uniform semiclassical treatment of Bieniek and Streeter [21] for the free-free Franck-Condon factors. Excellent agreement between the calculation and the experiment has been obtained in both shape and magnitude for the blue-wing $B \leftarrow X$ spectrum. The blue-wing spectrum with satellites SI and SII is interpreted as free-free transitions in the $B\ ^3 1 \leftarrow X\ ^1 0^+$ band of Hg-Ar. The satellite SII is the result of combined contributions from the inner and outer Condon-Points while the satellite SI results from the outer Condon point alone. In summing the contributions from all the angular-momentum components of the nuclear motion, the random-phase approximation employed in the generalized line-shape theories [8,10] is not valid for analyzing the satellite structures. The appearance of the satellites is due to the existence of a stationary phase-shift difference between the B and X state, i.e., a maximum of $\Delta\phi(l)$ as a function of the nuclear angular momentum l, which in turn is due to the existence of a maximum in the difference potential $V_B(R)-V_X(R)$.

ACKNOWLEDGMENTS

We wish to thank Dr. John B. West for suggestions and a careful reading of the manuscript. This work was partly supported by a Grant-in-Aid for Scientific Research (No. 06453014) from the Ministry of Education, Science, and Culture of Japan.

[1] H. Kuhn, Proc. R. Soc. London Ser. A **158**, 212 (1937).
[2] A. Michels, H. De Kluiver, and C. A. Ten Seldanm, Physica **25**, 1321 (1959).
[3] W. Behmenburg, Z. Naturforsch. Teil A **27**, 31 (1972).
[4] J. Losen and W. Behmenburg, Z. Naturforsch. Teil A **28**, 1620 (1973).
[5] J. F. Kielkopf and R. A. Miller, J. Chem. Phys. **61**, 3304 (1974).
[6] Z. Ben Lakhdar, D. Perrin, and R. Lennuier, J. Phys. (Paris) **37**, 831 (1976); **39**, 137 (1978).
[7] H. C. Petzold and W. Behmenburg, Z. Naturforsch. Teil A **33**, 1461 (1978).
[8] K. M. Sando and J. C. Wormhoudt, Phys. Rev. A **7**, 1889 (1973).
[9] K. M. Sando, Phys. Rev. A **9**, 1103 (1974).
[10] J. Szudy and W. E. Baylis, J. Quant. Spectrosc. Radiat. Transfer **15**, 641 (1975).
[11] K. Fuke, T. Saito, and K. Kaya, J. Chem. Phys. **81**, 2591 (1984).
[12] K. Yamanouchi, S. Isogai, M. Okunishi, and S. Tsuchiya, J. Chem. Phys. **88**, 205 (1988).
[13] M. Szajkowski, L. Krause, and R. Bobkowski, Phys. Rev. A **49**, 775 (1994).
[14] J. Koperski, J. B. Atkinson, and L. Krause, Chem. Phys. **186**, 401 (1994).
[15] D. Segal and I. D. Harris, J. Chem. Phys. **94**, 2713 (1991).
[16] X. Chen, K. Burnett, and D. M. Segal, J. Chem. Phys. **95**, 8124 (1991).
[17] C. J. K. Quayle, I. M. Bell, E. Takacs, X. Chen, K. Burnett, and D. M. Segal, J. Chem. Phys. **99**, 9608 (1993).
[18] K. Ueda, O. Sonobe, H. Chiba, and Y. Sato, J. Chem. Phys. **95**, 8083 (1991).
[19] T. Maeyama, H. Itoh, H. Chiba, K. Ohmori, K. Ueda, and Y. Sato, J. Chem. Phys. **97**, 9492 (1992).
[20] Y. Sato, in *Spectral Line Shapes*, Proceedings of the International Conference on Special Line Shapes, Toronto, 1994, edited by A. David May, J. R. Drummond, and E. Oks (AIP, 1994), Vol. 8, pp. 316–340.
[21] R. J. Bieniek and T. J. Streeter, Phys. Rev. A **28**, 3328 (1983).
[22] R. E. M. Hedges, D. L. Drummond, and A. Gallagher, Phys. Rev. A **6**, 1519 (1972).
[23] D. L. Drummond and A. Gallagher, J. Chem. Phys. **60**, 3426 (1974).
[24] A. Lurio, Phys. Rev. **140**, A1505 (1965).
[25] J. Tellinghuisen, A. Ragone, M. S. Kim, D. J. Auerbach, R. E. Smalley, L. Wharton, and D. H. Levy, J. Chem. Phys. **71**, 1283 (1979).
[26] P. S. Julienne, Phys. Rev. A **26**, 3229 (1982).
[27] R. J. Bieniek, Phys. Rev. A **15**, 1513 (1977); **23**, 2826 (1981).
[28] R. J. Le Roy, R. G. Macdonald, and G. Burns, J. Chem. Phys. **65**, 1485 (1976).
[29] F. J. Smith, Phys. Lett. **20**, 271 (1966).
[30] R. E. Olson, Phys. Rev. A **2**, 121 (1970).